

Characterization of ultrasound transmit-receive measurement systems in air

Comparison with prior work on piezoelectric elements in radial mode vibration

Renate Grindheim¹, Per Lunde^{1,2}, Magne Vestrheim¹

¹ University of Bergen, Department of Physics and Technology, P.O. Box 7803, N-5020 Bergen, Norway

² NORCE, Norwegian Research Centre AS, P.O. Box 6031, N-5898 Bergen, Norway
Contact email: renete@grindheim.net

Abstract

A system model is used, describing the voltage-to-voltage transfer function for an ultrasonic transmit-receive transducer pair based on simulations using a finite element model for piezoelectric transducers (FEMP). The piezoelectric ceramic elements used in this work are cylindrical Pz27 disks vibrating radially in air at room temperature and 1 atm, over a frequency range up to 300 kHz. Comparisons are made between measurements and simulations. Effects of uncertainties in alignment are examined, together with comparisons with prior work.

1 Introduction

Accurate modelling of ultrasonic measurement systems for characterization of gas is of interest in industrial and scientific applications. Examples include fiscal flow measurement for custody transfer of natural gas [1, 2], energy and quality measurement of gas [2–4], and sound velocity and absorption measurements [5, 6]. In the present work a “system model” of a transmit-receive measurement system refers to “a mathematical / numerical model aiming to describe the chain of electro-acoustic signal propagation through the system, from the electrical signal generator to the electrical recording equipment (e.g., an oscilloscope), via the piezoelectric transmit and receive transducers, the propagation medium, and possible transmit and receive cables/electronics” [7].

Various approaches have been used to describe transmit-receive ultrasonic measurement systems for fluids. This includes methods based on (i) the Mason model [or equivalent one-dimensional (1D) approaches] for thickness-mode transmitting and receiving transducers, combined e.g. with uniform piston [2, 8–14] or plane wave [15–20] type of radiation models; (ii) 1D “electroacoustic measurement (EAM) model” types of description [21–24]; and (iii) purely electrical transmission line system modelling [25]. More rigorous and accurate descriptions based on finite element modelling (FEM) have proven highly useful for ultrasonic system modelling, accounting for e.g. thickness-mode [26–30] and radial mode [5, 7, 31–36] transducers in such measurement setups.

The work presented here builds on prior work described in Refs. [5, 7, 31, 32, 34–36], using finite element modelling of an ultrasonic measurement system for air employing piezoelectric elements vibrating in their lower radial modes. Measurements and simulations of the frequency response of a voltage-to-voltage transmit-receive transfer function

are compared, including comparison with some recent work in this area [35, 36]. A second objective is to investigate and quantify measurement sensitivities to uncertainties in positioning and alignment of the transmitting and receiving piezoelectric elements in this setup.

2 Theory

The experimental measurement setup used in the present work is described in Section 3.1. A system model based on this setup is used. This was first introduced by [31, 32], cf. [7], and further developed by [34–36].

2.1 System model

The system model illustrated in Figure 1 shows the different components included in the measurement setup as linear blocks where transfer functions relate the signal going from one block to another in the frequency domain. The system model consists of two cylindrical, 10 mm × 2 mm, Pz27 piezoelectric ceramic disks in radial mode vibration in air, where the transmitting disk, T_x , is coupled to the transmitting electronics (signal generator, oscilloscope and cables), and the receiving disk, R_x , is coupled to the receiving electronics (amplifier, filter, cables and oscilloscope). The two disks are mounted parallel (with respect to the xy -plane, cf. Figure 3a) at a separation distance d along the z -axis.

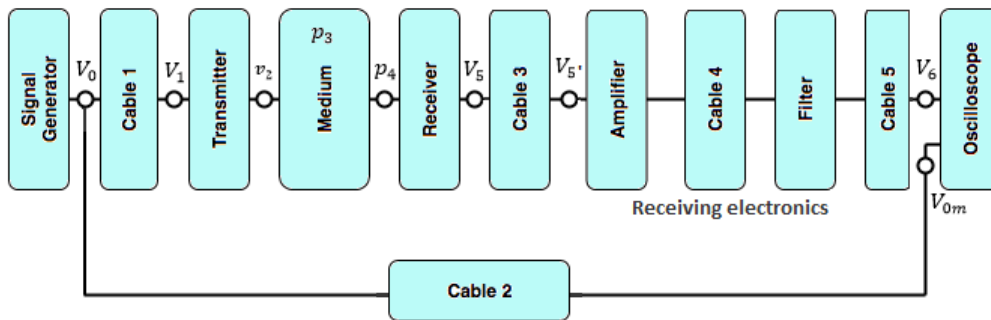


Figure 1: Block diagram representation of the system model used in the present work.

The voltage signals $V_6(t)$ and $V_{0m}(t)$ measured at the oscilloscope are Fourier transformed as described in [36], giving the respective spectral components $V_6(f)$ and $V_{0m}(f)$, where t is the time and f is the frequency. For these spectral components a monochromatic time dependency $e^{i\omega t}$ is assumed and suppressed. At angular frequency $\omega = 2\pi f$ $V_0(f)$ is the output voltage spectral component generated by the signal generator and $V_{0m}(f)$ is the output voltage spectral component measured in Channel 1 on the oscilloscope. $V_1(f)$ is the input voltage spectral component at the transmitting disk, T_x . v_2 is the spectral component of the particle velocity at the center of the front surface of T_x . p_3 is defined in [32] and not discussed in the current work. p_4 is the on-axis spectral component of the free-field pressure at the front of R_x . $V_5(f)$ is the output voltage spectral component at R_x , and $V_{5'}(f)$ is the output voltage spectral component at the amplifier. $V_6(f)$ is the input voltage spectral component measured and terminated in Channel 2 on the oscilloscope.

2.2 Transfer functions

The voltage spectral components $V_6(f)$ and $V_{0m}(f)$ are divided to obtain the voltage-to-voltage transfer function of the complete signal chain as defined in Equation (2.1) in [34] with the receiving electronics treated as in Equation (2.64) in [36], i.e.

$$H_{0m6}^{VV}(f) \equiv \frac{V_6(f)}{V_{0m}(f)} = \frac{V_1(f)}{V_{0m}(f)} \cdot \frac{V_{5open}(f)}{V_1(f)} \cdot \frac{V_{5'}(f)}{V_{5open}(f)} \cdot \frac{V_6(f)}{V_{5'}(f)}. \quad (1)$$

The various transfer functions used in Eq. (1) are described in the following. The open-circuit voltage-to-voltage transfer function describing the sound propagation from T_x to R_x at lossless conditions in the air medium is defined as equation (2.20) in [31],

$$H_{15open}^{VV}(f) = |H_{15open}^{VV}(f)|e^{i\theta_{15open}} \equiv \frac{V_{5open}}{V_1}, \quad (2)$$

where V_{5open} is the open-circuit voltage at R_x . $|H_{15open}^{VV}(f)|$ is the magnitude and θ_{15open} the phase of this transfer function. The phase can be decomposed into a slowly varying phase and a plane wave component, cf. Equation (2.100) in [34] and Equation (2.14) in [35]. The slowly varying phase is then given by

$$\theta_{15open}^{slow} = \theta_{15open} + kd, \quad (3)$$

where $k = \omega/c$ is the wave number and c is the speed of sound in air.

The transfer function relating the measured voltage at Channel 1 on the oscilloscope to the voltage at T_x , H_{0m1}^{VV} , is defined as equation (2.5) in [35]

$$H_{0m1}^{VV}(f) = \frac{V_1(f)}{V_{0m}(f)}. \quad (4)$$

The transfer functions $H_{5open5'}^{VV}$, describing the influence of the electrical load from cable 3 and the receiving electronics on the output voltage from R_x , and $H_{5'6}^{VV}$, describing the receiving electronics including cables 4 and 5, are defined as [36],

$$H_{5open5'}^{VV}(f) = \frac{V_{5'}(f)}{V_{5open}(f)} \quad (5)$$

and

$$H_{5'6}^{VV}(f) = \frac{V_6(f)}{V_{5'}(f)}, \quad (6)$$

respectively.

2.3 Simulated transfer function H_{15open}^{VV}

The simulated lossless open-circuit transfer function H_{15open}^{VV} is calculated by assuming spherical reciprocity and using the simulated far-field axial pressure $p_{ff} = p_4(z_{ff})$, where $z_{ff} = 1000$ m is used, extrapolating it to the desired distance, d . This model assumes identical transducers and does not include losses in the medium or diffraction effects caused by the distance, d , being in the near-field of the transducers. The lossless open-circuit transfer function is then given as Equation (2.52) in [35],

$$H_{15open}^{VV}(f) = \frac{Z_T p_4^2(z_{ff}) 2z_{ff}^2}{i\rho d f} e^{ik(2z_{ff}-d)}, \quad (7)$$

where the input electrical impedance of T_x , Z_T , and the far-field pressure, $p_4(z_{ff})$, is simulated using finite element modelling (FEMP) [37], and ρ is the density of the medium.

2.4 Measured transfer function H_{15open}^{VV}

In order to obtain a lossless open-circuit transfer function, $H_{15open}^{VV}(f)$, from measurements, corrections are made for attenuation in the medium and near-field effects caused by diffraction due to the finite sizes of T_x and R_x . The attenuation correction factor, C_α , is found by accounting for attenuation due to the classical absorption of sound in air, α_{cl} , rotational motion of the air molecules, α_{rot} , vibrations of oxygen molecules, $\alpha_{vib,O}$ and vibration of nitrogen molecules, $\alpha_{vib,N}$. These are calculated according to [38] with the theory for implementation in the system model described in [32]. The diffraction correction C_{dif} , is found by using a baffled piston diffraction correction factor as in [31–36], where the diffraction correction is calculated according to Khimunin's model [39, 40].

H_{0m1}^{VV} and $H_{5open5'}^{VV}$ are estimated using transmission line models as proposed in [34]. $H_{5'6}^{VV}$ is found by measuring the transfer function of the receiving electronics including cables 4 and 5, by coupling the signal generator to an attenuator and then directly into the receiving electronics, bypassing the transmitting and receiving transducer completely, as in [36].

From Equation 1-6 and the corrections mentioned above, the lossless transfer function $H_{15open}^{VV}(f)$ is calculated as

$$H_{15open}^{VV}(f) = \frac{H_{0m6}^{VV}(f)}{H_{0m1}^{VV}(f) H_{5open5'}^{VV}(f) H_{5'6}^{VV}(f)} C_\alpha C_{dif}. \quad (8)$$

3 Methods

The experimental setup has been largely kept as used by [34–36] with only minor changes such as the lengths of cables 4 and 5, and the different instruments having been moved due to a renovation at the lab in 2017.

3.1 Experimental Setup

The two piezoelectric disks are mounted in air on positioning stages (Physik Instrumente GmbH&Co, Germany). T_x is connected to a PI linear positioning stage (PI M-531.DG [41]), allowing movement in the z -direction, and to a PI rotational stage (PI M-037.PD [42]) for rotation about the x -axis, cf. Figure 3. R_x is connected to a PI linear position stage (PI M-535.22 [43]) moving in y -direction, and can be rotated about the x -axis by loosening a screw at the top of the rod it is connected to, allowing it to be turned. Two lasers, mounted on a rod, can be placed between the two disks in order to measure (i) the alignment and (ii) the distance, d (cf. Figure 3b). In this work the distance $d = 0.50$ m, is used.

An Agilent 33220A function generator is used to generate the input signal at desired voltage over the frequency range 30 - 300 kHz. The signal $V_{0m}(t)$ is then measured using

a Tektronix DPO3012 digital oscilloscope. R_x is connected to a Brüel&Kjær 2636 amplifier and a Krohn-Hite 3940A digital filter before the signal terminates in the Tektronix DPO3012 digital oscilloscope and $V_6(t)$ is measured. The cables used to connect the instruments (cables 2, 4 and 5) are coaxial cables of type RG-58, with lengths $l_2 = 0.280$ m, $l_4 = 0.475$ m and $l_5 = 1.470$ m. The cables used to connect the oscilloscope to T_x and R_x to the amplifier (cables 1 and 3, respectively) are coaxial cables of type RG-178 B/U, with length $l_1 = 2.970$ m and $l_3 = 2.975$ m, respectively. For the present work the piezo-electric disk elements used are denoted elements 7 and 13, as transmitter and receiver, respectively. This is the same as used in [36], whereas [35] used elements 4 and 13, cf. the comparisons made in Section 4.2.



Figure 2: Experimental setup in the acoustics laboratory.

3.2 Alignment of the transmitter, T_x , and receiver, R_x .

The disks are soldered onto partially twisted pairs cables, shielded with aluminium foil, mounted in a Faraday cage, cf. Figures 2 and 3b. The aim is to have the disks centred on the z -axis and place them parallel to the xy -plane as shown in Figure 3. This is done using two high precision Keyence lasers [35], measuring differences in the $+$ and $-$ z -direction to measure the position of the disks, and the high precision translation stages from Physik Instrumente, cf. Section 3.1, to position the disks.

Firstly the disks are roughly placed on the z -axis by adjusting R_x in x - and y -direction so that the two laser beams point to the x marking the center on each of the disks. This mark has a finite size, so the laser is moved to the top, bottom (vertically) and side edges (horizontally) of the disks to see if these are aligned. Adjustments are made by moving R_x in x - and y -direction if necessary.

When the disks are both centred on the z -axis and aligned vertically and horizontally, the rotational alignment is investigated. For rotation about the y -axis this is done by moving the laser to the top and the bottom of T_x , noting the distance from the laser to the disk in both positions and subtracting them to find the difference. This is referred to as uncertainty in the alignment caused by rotation about the y -axis. If alignment is not satisfactory the disk is moved by a light touch at the bottom of the disk, continuously monitoring the position on the laser display until the desired deviation about the y -axis is acquired. This procedure is then repeated for R_x .

For rotation about the x -axis the laser is placed on one of the furthest horizontal sides

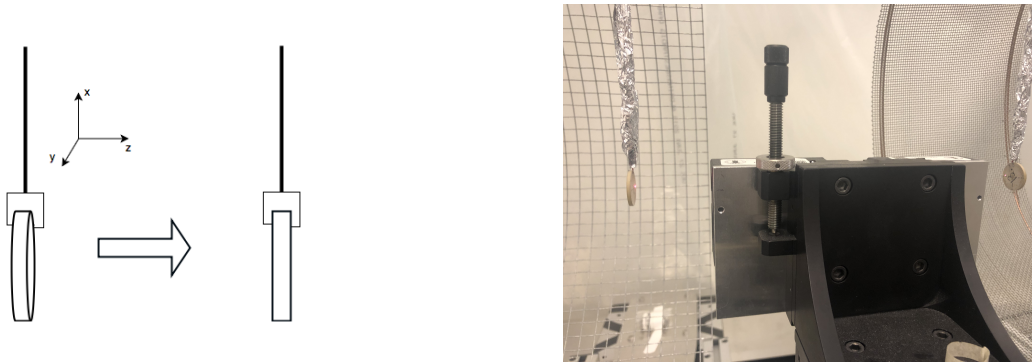


Figure 3: Sketch of a) the mounting of the piezoelectric ceramic disks and b) aligning of the disks using laser.

of the disk. The uncertainty in alignment is found by measuring at the two horizontal sides of the disk and subtracting the two distances to find the difference. For T_x corrections are now made by using the rotation stage mentioned in Section 3.1. For R_x a light touch or a screw at the top of the mounting rod allows for the rod and the disk to be rotated and is used to correct its positioning.

The process is repeated several times, to check that corrections in one direction did not affect the deviation or uncertainty in alignment in another direction, until satisfactory alignment is achieved.

Lastly the positioning stage in z -direction is used to position the front of the transmitting disk at the separation distance $z = d$ and the front face of the receiver is placed at $z = 0$. The combined standard uncertainty for the separation distance, d , as claimed in Section 7.1.1 in [35], is $40 \mu\text{m}$ at a coverage factor $k = 1$.

The small and bright red/white area on each piezoelectric disk in Figure 3b shows the "footprint" of the laser beam on the disk, for a given position of the laser, at which a distance measurement is made. As described above, the laser beam is then traversing over the disk surface in a "diametrical cross formation" (in the x - and y -directions), to get a distribution of distance measurements over this cross formation.

4 Results

4.1 The influence of accuracy in alignment

In [35] the tolerated uncertainty in alignment of the disks in the xy -plane was given as $10 \mu\text{m}$ or less, whereas [36] allowed for uncertainties up to $100 \mu\text{m}$. Therefore the effect of different alignment uncertainty is investigated by aligning the disks to different degrees of accuracy and observing how this affects the transfer function, H_{0m6}^{VV} . The accuracies chosen were $500 \mu\text{m}$, $50 \mu\text{m}$ and $10 \mu\text{m}$. The results are shown in Figure 4.

For the first two peaks, associated with the fundamental radial mode R_1 , there is little to no change in the magnitude of the transfer function H_{0m6}^{VV} , for all three accuracies. At the second pair of peaks, associated with the second radial mode R_2 , there is no noticeable change in the magnitude for alignment to the degree of $50 \mu\text{m}$ and $10 \mu\text{m}$. However, the measurement with $500 \mu\text{m}$ uncertainty in the alignment shows a decrease in magnitude of almost 5 dB compared to the measurements with $50 \mu\text{m}$ and $10 \mu\text{m}$ misalignment.

The effect of misalignment in the slowly varying phase will be investigated further in

[44].

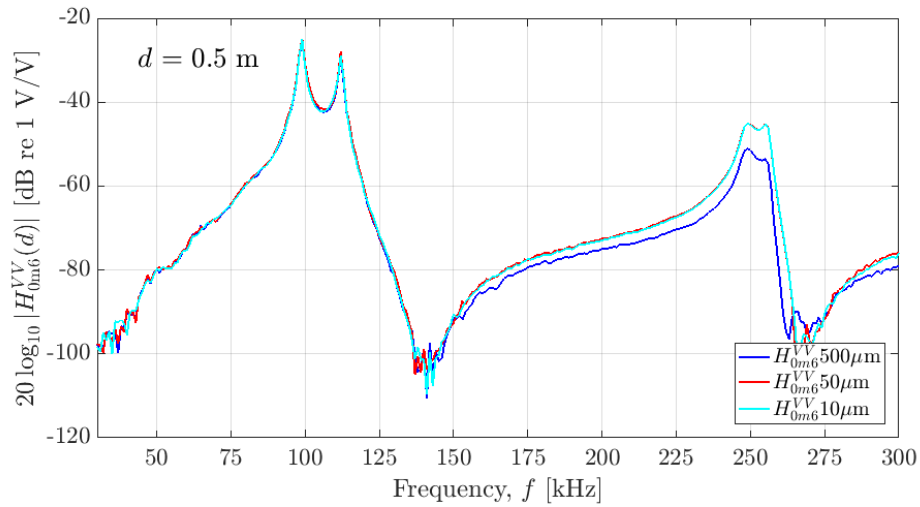


Figure 4: Measurements of the magnitude of the transfer function H_{0m6}^{VV} for different accuracies in rotational alignment of the disks.

4.2 Comparison with prior work

Measurements of the open-circuit transfer function H_{15open}^{VV} as compared to prior work [35, 36] is shown in Figure 5. Comparisons of the slowly varying phase is also of interest and will be further discussed in [44].

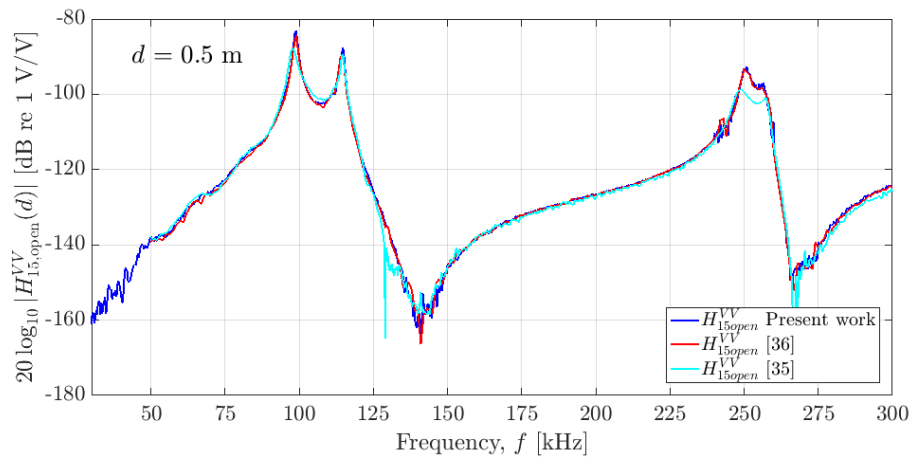


Figure 5: Measurements of the magnitude of the transfer function H_{15open}^{VV} as compared with prior work [35, 36].

It should be noted that the receiving disk used by Hagen [36] and in the present work are not the same as used by Andersen [35], and the calculation of the receiving electronics transfer function, $H_{5/6}^{VV}$, differ slightly as the filter is coupled in series after the amplifier in the present work and [36], whereas [35] coupled the filter between the input and output sections of the amplifier. The signal generator voltage settings used for measurements vary for the different frequencies, cf. [7]. At R_1 the voltage settings used are 0.1 V for the present work and 1 V for [35] and [36]. For R_2 the voltage settings used are 0.1 V in the present work and [36] and 1 V in [35]. For all other frequencies the voltage setting is 10

V in the current work, [35] and [36]. The frequency steps used in the present work, [35] and [36], are 300 Hz, 500 Hz and 1 kHz, respectively.

In the frequency range 30 - 80 kHz the measurements in the present work reveal a clear undulation pattern, which is also present in the measurements presented in [7, 31, 32] (but not as clear in [35, 36]). In [33] these are shown to be due to side radiation from T_x .

For the magnitude of H_{15open}^{VV} at the first peak associated with R_1 , the deviations of the present work are about 4.5 and 1 dB relative to [35] and [36], respectively. For the second peak associated with R_1 the deviations of the present work are 1.5 and 1 dB, relative to [35] and [36].

Similarly, for R_2 , the corresponding deviations of the present work at the first peak are 6 and 1 dB, relative to [35] and [36]. At the second peak associated with R_2 , the deviations of the present work relative to [35] and [36] are 4 and 1 dB, respectively.

The oscillations in the magnitude of the current work and [36] about 240 kHz is likely due to the switch from 10 V input voltage to 0.1 V input voltage for the R_2 frequency range. This will be investigated further in [44].

With respect of the frequencies for the two peaks associated with R_1 and the first peak associated with R_2 , the corresponding deviations of the present work relative to [35] and [36] are about 1 kHz, typically. At the second peak associated with R_2 , the deviations of the present work relative to [35] and [36] are 3.5 and 2 kHz, respectively.

Figure 6 shows simulations of the magnitude and the slowly varying phase of the transfer function H_{15open}^{VV} , as compared to prior work [35, 36], calculated using two different finite element software tools: FEMP [37] and COMSOL [45].

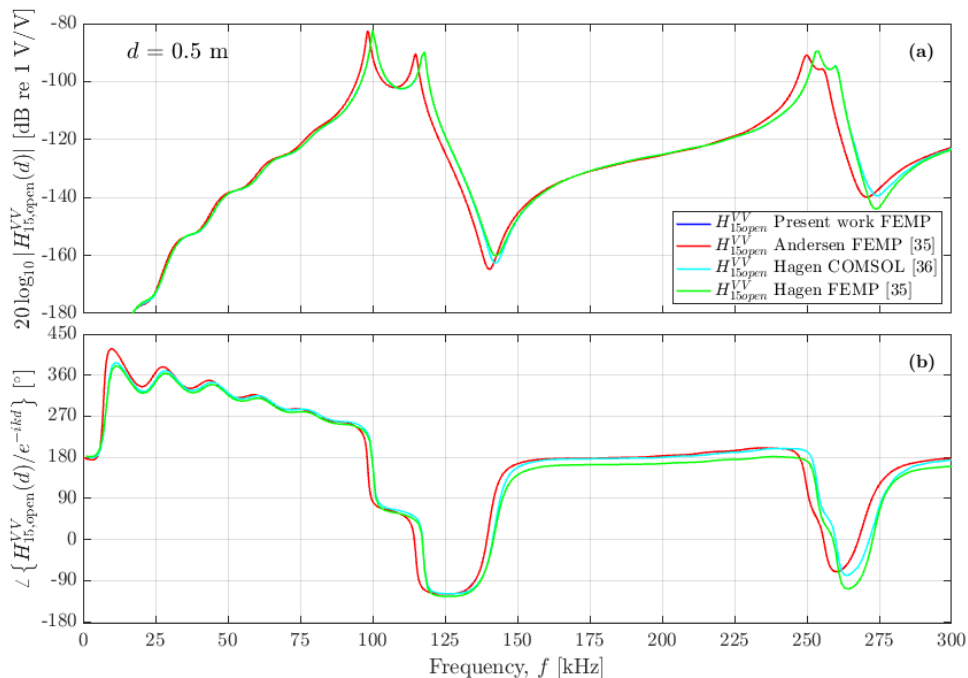


Figure 6: Simulated transfer function H_{15open}^{VV} for a) the magnitude and b) the slowly varying phase, θ_{15open}^{slow} , as compared with prior work.

The same material parameters, piezoelectric disk dimensions, software (FEMP) and finite element mesh, are used for simulations in the current work and by Andersen [35].

Therefore these curves are identical, cf. Figure 6. The simulations done in COMSOL and FEMP by Hagen [36] differ from the current work and Andersen [35]. There is a lower magnitude found in the present work and [35] compared to [36] for the first and second peak associated with R_1 , of about 0.3 dB and 0.7 dB, respectively. For the two peaks associated with R_2 the deviations are about 0.6 dB and 1 dB, respectively. There is a lower frequency for the two peaks associated with R_1 for the present work and [35] as compared to [36], and the differences are about 2 and 3 kHz, respectively. For the two peaks associated with R_2 , the differences are about 3 and 5 kHz, respectively.

5 Conclusions and further work

The sensitivity of the transfer function $H_{15open}^{VV}(f)$ with respect to rotary alignment about the y - and x -axes is investigated. It is found that a rotary misalignment less than 50 μm does not significantly influence on $|H_{0m6}^{VV}(f)|$. However a rotary misalignment $\approx 500 \mu\text{m}$ reduces $|H_{0m6}^{VV}(f)|$ significantly, especially for R_2 , at which there is a decrease of approximately 5 dB.

Comparisons with prior experimental measurements show some deviations from [35] and [36]. The largest deviations are found in the first peak associated with R_1 and at the two peaks associated with R_2 . For R_2 an input voltage of 1 V was applied by [35], whereas [36] used 0.1 V, as in the current work. The low voltage of 0.1 V at R_2 and $H_{5/6}^{VV}(f)$ as defined in [36] may explain some of the deviations and will be further investigated in [44].

Comparisons with prior simulations [35, 36] show deviations from [36]. Both higher frequency for the four peaks of R_1 and R_2 (2, 3, 3 and 5 kHz, respectively) and larger magnitude at R_2 (0.6 and 1 dB, for the two peaks) are observed in the simulations of [36] as compared the current work and [35]. The simulations by [36] using FEMP and COMSOL show some deviation, especially above R_2 . The material data, the dimensions of the simulated piezoelectric disk elements chosen and the finite element mesh chosen may contribute to the observed deviations. This will be investigated further in [44].

6 Acknowledgements

The present work is part of an ongoing master work on the sound field and measurement system modelling using piezoelectric elements vibrating in air, due by June 2019 [44]. The following persons are acknowledged for guidance and assistance: Espen Storheim, Andreas Hagen, Magnus Rentch Ersdal and Kenneth K. Andersen.

References

- [1] ISO 17089-1:2010, "Measurement of fluid flow in closed conduits. Ultrasonic meters for gas. part 1: Meters for custody transfer and allocation measurement," *International Organization for Standardization, Geneva, Switzerland*, 2010.
- [2] P. Lunde, K.-E. Frøysa, R. A. Kippersund, and M. Vestrheim, "Transient diffraction effects in ultrasonic meters for volumetric, mass and energy flow measurement of natural gas." 21st International North Sea Flow Measurement Workshop, Tønsberg, Norway, 28-31 Oct., 2003.

- [3] K.-E. Frøysa, P. Lunde, A. Paulsen, and E. Jacobsen, "Density and calorific value measurement of natural gas using ultrasonic flow meters. Results from testing on various north sea gas field data." 24th International North Sea Flow Measurement Workshop, St. Andrews, Scotland, 24-27 Oct., 2006.
- [4] M. Farzaneh-Gord, A. Arabkoohsar, and R. N. N. Koury, "Novel natural gas molecular weight calculator equation as a function of only temperature, pressure and sound speed," *Journal of Natural Gas Science and Engineering*, vol. 30, pp. 195–204, 2016.
- [5] P. Norli, "Sound velocity cell for gas characterizsation". PhD thesis, University of Bergen, Department of Physics and Technology, Bergen, Norway, 2007.
- [6] P. Lunde, P. Norli, M. Vestrheim, and R. Kippersund, "Precision sound velocity cell as reference for gas quality measurement in ultrasonic flow meters. Preliminary results using two candidate methods with argon at low pressure." Proc. 30th Scand. Symp. Phys. Acoust., Geilo, Norway, Jan. 28-31, 2007.
- [7] R. Øyerhamn, E. N. Mosland, E. Storheim, P. Lunde, and M. Vestrheim, "Finite element modeling of ultrasound measurement systems for gas. Comparison with experiments in air," *J. Acoust. Soc. Am.*, vol. 144(4), pp. 2613–2625, 2018.
- [8] P. Stepanishen, "Pulsed transmitt/receiver response of ultrasonic piezoelectric transducers," *J. Acoust. Soc. Am.*, vol. 69(6), pp. 1815–1827, 1981.
- [9] A. Lygre, M. Vestrheim, P. Lunde, and V. Berge, "Numerical simulation of ultrasonic flowmeters," *Proc. 1987 Ultrasonics International, Butterworth Scientific Ltd., Guildford, UK*, pp. 196–201, 1981.
- [10] D. A. L. Collie and M. A. Player, "Extended computer method for predicting the transient response of ultrasound NDT probes," *Ultrasonics*, vol. 27, pp. 141–149, 1989.
- [11] S. Vervik, "Transitt-tidsbestemmelse for ultralyd strømningsmetre. Nullstrømningsforhold [Transit time detection for ultrasonic flow meters at zero flow conditions]," Master's thesis, Dept. of Physics, Univ. of Bergen, Norway, 1995. (In Norwegian).
- [12] M. Willatzen, "Ultrasound transducer modeling - Receieved voltage signals and the use of half-wavelength window layers with acoustic coupling layers," *IEEE Trans. Ultrason. Ferroelectr. Freq. Control*, vol. 46(5), pp. 1164–1174, 1999.
- [13] S. Vervik, "Methods for characterization of gas-coupled ultrasonic sender-receiver measurement systems". PhD thesis, University of Bergen, Department of Physics, Bergen, Norway, 2000.
- [14] M. Willatzen, "Ultrasound transducer modeling - General theory and applications to ultrasound reciprocal systems," *IEEE Trans. Ultrason. Ferroelectr. Freq. Control*, vol. 48(1), pp. 100–112, 2001.
- [15] E. Papadakis, "Ultrasonic transducer evaluation in five "domains": time, space, frequency, surface motion, and theory," *IEEE Trans. Ultrason. Symp., Phoenix, Arizona, USA, Oct. 26-28*, pp. 104–112, 1977.

- [16] G. Low, "A simple computer method for predicting the transient response of ultrasonic NDT probes," *NDT International*, vol. 13(6), pp. 285–290, 1980.
- [17] G. Hayward and M. Jackson, "Discrete-time modeling of the thickness mode piezoelectric transducer," *IEEE Trans. Son. Ultras.*, vol. 31(3), pp. 137–150, 1984.
- [18] G. Hayward, M. Jackson, and T. Durrani, "A systems model of the thickness mode piezoelectric transducer," *J. Acoust. Soc. Am.*, vol. 76(2), pp. 369–382, 1984.
- [19] K. Yamaguchi, H. Yagami, and T. Fuji, "New method of time domain analysis of the performance of multilayered ultrasonic transducers," *IEEE Trans. Ultrason., Ferroelect., Freq. Contr.*, vol. 33(6), pp. 669–678, 1986.
- [20] P. Wilcox, R. Monkhouse, P. Cawley, M. Lowe, and B. Auld, "Development of a computer model for an ultrasonic polymer film transducer system," *NDT & E International*, vol. 31(1), pp. 51–64, 1998.
- [21] C. Dang, L. W. Schmerr, and A. Sedov, "Modeling and measuring all the elements of an ultrasonic nondestructive evaluation system I: Modeling foundations," *Res. Nondestr. Eval.*, vol. 14(3), pp. 141–176, 2002.
- [22] C. Dang, L. W. Schmerr, and A. Sedov, "Modeling and measuring all the elements of an ultrasonic nondestructive evaluation system II: Model-based measurements," *Res. Nondestr. Eval.*, vol. 14(4), pp. 177–201, 2002.
- [23] L. W. Schmerr and S. Song, "Ultrasonic nondestructive evaluation systems: Models and measurements." Springer, London, UK, 2007.
- [24] L. W. Schmerr and A. Sedov, "Ultrasonic measurement models for contact testing with bulk waves, surface waves, and plate waves," *Res. Nondestr. Eval.*, vol. 22, pp. 129–146, 2011.
- [25] J. van Deventer, T. Lofqvist, and J. Delsing, "Pspice simulation of ultrasonic systems," *IEEE Trans. Ultrason., Ferroelect., Freq. Contr.*, vol. 47, pp. 1014–1024, 2000.
- [26] P. Lunde, R. A. Kippersund, and M. Vestrheim, "Signal modeling using the FLOSIM system model in ultrasonic instrumentation for industrial applications." Proc. Norw. Symp. Signal Proc. (NORSIG 2003), Bergen, Norway, Oct. 6, 2003.
- [27] M. Bezděk, H. Landes, A. Rieder, and R. Lerch, "A coupled finite-element, boundary-integral method for simulating ultrasonic flowmeters," *IEEE Trans. Ultrason., Ferroelect., Freq. Contr.*, vol. 54(3), pp. 636–646, 2007.
- [28] M. Bezděk and B. Tittman, "Dispersion analysis of a three-layered waveguide with finite element and matrix methods," *Acta Acustica united with Acustica*, vol. 94, pp. 792–806, 2008.
- [29] M. Bezděk, "Numerical modeling of ultrasonic flowmeters." VDM Verlag Dr. Müller GmbH & Co KG, Saarbrücken, Germany, 2008.
- [30] L. Ge, X. Wang, and C. Jin, "Numerical modeling of PZT-induced Lamb wave-based crack detection in plate-like structures," *Wave Motion*, vol. 51, pp. 867–885, 2014.

- [31] R. Hauge, “Finite element modeling of ultrasound measurements for gas. Comparison with experiments in air,” Master’s thesis, University of Bergen, Department of Physics and Technology, Bergen, Norway, 2013.
- [32] E. Mosland, “Reciprocity calibration method for ultrasonic piezoelectric transducers in air,” Master’s thesis, University of Bergen, Department of Physics and Technology, Bergen, Norway, 2013.
- [33] E. Storheim, “*Diffraction effects in the ultrasonic field of transmitting and receiving circular piezoceramic disks in radial mode vibration. FE modelling and comparison with measurements in air*”. PhD thesis, University of Bergen, Department of Physics and Technology, Bergen, Norway, 2015.
- [34] A. A. Søvik, “Ultrasonic measurements systems for gas. Finite element modeling compared with measurements in air,” Master’s thesis, University of Bergen, Department of Physics and Technology, Bergen, Norway, 2015.
- [35] K. K. Andersen, “Reciprocity calibration of ultrasonic piezoelectric disks in air,” Master’s thesis, University of Bergen, Department of Physics and Technology, Bergen, Norway, 2015.
- [36] A. Hagen, “Ultrasonic measurement system with diffraction correction for gas,” Master’s thesis, University of Bergen, Department of Physics and Technology, Bergen, Norway, 2017.
- [37] J. M. Kochbach, “*Finite element modeling of ultrasonic piezoelectric transducers*”. PhD thesis, University of Bergen, Department of Physics and Technology, Bergen, Norway, 2000.
- [38] ANSI S1.26, “Method for calculation of the absorption of sound by the atmosphere,” *American National Standards Institute, New York*, vol. (R2009), pp. 2613–2625, 1995.
- [39] S. Khimunin, “Numerical calculation of the diffraction correction for the precise measurement of ultrasound absorption,” *Acta Acustica united with Acustica*, vol. 27(4), pp. 173–181, 1972.
- [40] S. Khimunin, “Numerical calculation of the diffraction corrections for the precise measurement of ultrasound phase velocity,” *Acta Acustica united with Acustica*, vol. 32(3), pp. 192–200, 1975.
- [41] Physik Instrumente (PI) GmbH & Co. KG, *Datasheet M-511, M-521, M-531, High-Precision Linear Stage*. Karlsruhe, Germany, January 15 2018.
- [42] Physik Instrumente (PI) GmbH & Co. KG, *User Manual MP 34E Rotation Stages M-038, M-035 Series*, Karlsruhe, Germany, August 28 2002.
- [43] Physik Instrumente (PI) GmbH & Co. KG, *MP 33E User Manual, M-5x1 Series Linear Positioning Stages*. Karlsruhe, Germany, September 20 2004.
- [44] R. Grindheim, Master’s thesis, University of Bergen, Department of Physics and Technology, Bergen, Norway, 2019, (In preparation).
- [45] COMSOL AB, *COMSOL Multiphysics version 4.2a Manual*.